# Collisional heating and adiabatic expansion of warm dense matter with intense relativistic electrons

J. E. Coleman and J. Colgan

Phys. Rev. E **96**, 013208 — Published 13 July 2017

DOI: 10.1103/PhysRevE.96.013208

# Collisional heating and adiabatic expansion of WDM with intense relativistic electrons

J.E. Coleman and J. Colgan
*Los Alamos National Laboratory, Los Alamos, NM 87545, USA.*
(Dated: June 9, 2017)

Adiabatic expansion of a warm dense Ti plasma has been observed after isochorically heating a 100-$\mu$m-thick Ti foil with a ∼100-ns-long intense relativistic electron bunch at an energy of 19.8 MeV and current of 1.7 kA. The expansion fits well with the analytical point source solution [1–3]. After 10 J is deposited and the plasma rapidly expands out of the warm dense phase, a stable degenerate plasma (T ∼ 1.2 eV) with a $n_e > 10^{17}$ cm$^{-3}$ is measured for > 100 ns. This is the first temporal measurement of the generation and adiabatic expansion of a large volume ($3\times10^{-4}$ cm$^3$) of warm dense plasma isochorically heated by intense monochromatic electrons. The suite of diagnostics is presented, which includes time resolved plasma plume expansion measurements on a single shot, visible spectroscopy measurements of the emission and absorption spectrum, measurements of the beam distribution, and plans for the future.

PACS numbers: 07.60.Rd, 52.50.Sw, 52.40.Mj, 52.25.Jm, 52.25.Os, 52.70.Kz

## I. INTRODUCTION

Warm dense matter (WDM) is a region in temperature-density space ranging from: $0.1 < T_e$ (eV) $< 10$ eV and $10^{22} < n_e$ (cm$^{-3}$) $< 10^{24}$ for most metals that is not described well by normal condensed matter or weakly coupled plasma theory. WDM has been produced by multiple mechanisms through shock heating with photons, magnetic compression, or collisional heating with particle beams. High power lasers with 6 ns pulses of 300-450 J were used to shock heat 300 $\mu$m of LiH, to 2 eV, $10^{23}$ cm$^{-3}$ [4, 5] and a stepped 13.5 kJ, 3 ns pulse profile was used to shock heat a 70 $\mu$m CH shell to 8 eV, $10^{24}$ cm$^{-3}$ [6]. Free electron lasers (FEL) have been explored as heating probes also, the LCLS 8.9 keV, 60 fs, XFEL provided 1 mJ of heat to 0.5 $\mu$m of Ag to achieve 10 eV and calculated densities $10^{24}$ cm$^{-3}$ with two different equation-of-state (EOS) models [7]. The FLASH UV FEL delivered 10-30 $\mu$J in 25 fs to a 20 $\mu$m spot to heat Al to 0.8 eV [8]. Laser heating experiments have traditionally been used to validate the Hugoniot curves [9].

Magnetic compression produced shock heating with both Z and X-pinches. X-ray Thomson measurements on the Z-facility indicate shock compression at 20 MA of carbon foams to a temperature of 4.3 eV and $n_e \sim 10^{20}$ cm$^{-3}$ [10]. A two-wire X-pinch drove 40-$\mu$m of Al with 150 kA to produce 10-30 eV coronal plasmas with $n_e < 10^{20}$ cm$^{-3}$ [11]. These measured densities were slightly below the warm dense phase.

Particle beam driven WDM has been investigated by several means. Research with Uranium ions at GSI have proposed collisional heating by delivering $5\times10^{11}$ $U^{28+}$ ions accelerated to 400 MeV/u (95.2 GeV) in a 350-$\mu$m-spot and 70 ns pulse to achieve 4.2 eV temperatures in solid hydrogen [12, 13]. They demonstrated heating of a 100-$\mu$m-thick W target to 0.56 eV with $U^{74+}$ ions accelerated to 350 MeV/u (83.3 GeV) in a 120 ns bunch [14]. Intense light ions from the NDCX-I facility [15] have been used to heat Au targets to 0.38 eV [16] and 0.27 eV [17] using a 4 $\mu$s bunch of 0.3 MeV, 30-mA $K^+$ ions; no density was measured in either case. The NDCX-II accelerator provided 1.2 MeV $Li^+$ ions with 1.6 nC of charge in a 2 ns pulse [18] and more recently 15 nC of $He^+$ ions [19] have been used to begin heating experiments on 300-nm-thick Sn [20]. None of these experiments have successfully measured a density or an expansion rate.

Intense short pulsed lasers have also been used to accelerate ions. A 60 J, 1 ps laser heated a 20-$\mu$m-thick Au foil to produce 60 nC protons, with a peak energy of 17 MeV, which deposited 180 mJ in C heating it to 0.39 eV [21]. The 80 J, 650 fs Trident laser accelerated ∼140 MeV $Al^+$ ions from 110-nm-thick Al foil onto a 10-$\mu$m-thick Au and 15-$\mu$m-thick C hybrid interface. Expansion speeds of 6.7 $\mu$m/ns and 7.5 $\mu$m/ns were measured for C and Au leading to inferred temperatures of 1.7 and 5.5 eV [22, 23] using the RAGE code [24] and available SESAME tables[25]. Again these experiments did not measure a plasma density. To date there has been no measurement of plasma density from collisional, isochoric heating of a solid target.

Intense relativistic electron beam-target interactions were studied nearly two decades ago. The interactions of intense electrons with plasma densities exceeding the beam density [26–28] lead to the development of wakefield acceleration techniques for bunches < 100 ps. Experiments explored time dependent focusing effects through streaked measurements of Cherenkov light produced by the beam at focus [29]. Simple gated images of the plasma plume were made on the ETA facility but were not quantitatively characterized [30]. LSP was used to investigate the beam target interaction [31, 32] by characterizing the gas desorption of the contaminant layer and the backstreaming velocity using particle-in-cell (PIC) techniques; dense plasmas and hydro motion were not considered at the time. A detailed model of the hydrodynamic expansion of the particle beam heated foil has been attempted with hydro codes LASNEX[30, 33] and more recently RAGE[24, 34] in addition to a PIC-fluid hybrid model in LSP[35]. The integration of these

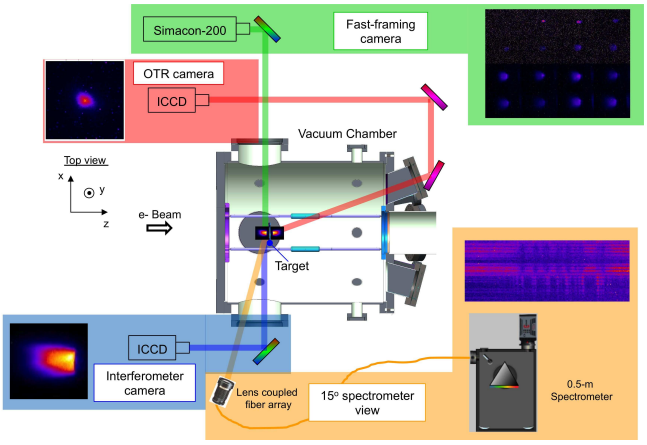


FIG. 1: View of the vacuum test section in which the expanding warm dense plasma is diagnosed. The target location, optical diagnostic layouts, lines of sight, and sample data sets are shown. The imaging station for OTR is shaded in red, the imaging station for the interferometer camera is shaded in blue, the fast-framing camera is shaded in green, and the $15^o$ upstream spectrometer is shown in orange. (An orthogonal visible spectrometer is not shown).

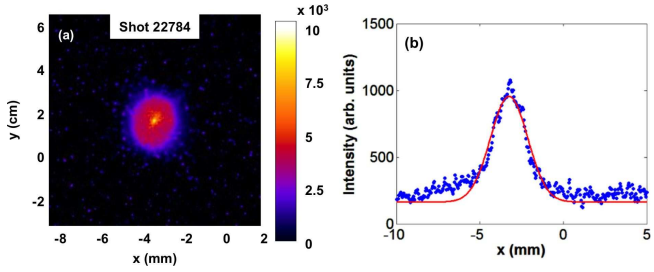


FIG. 2: (a)10 ns gated OTR image of the beam distribution on the foil, 20 ns after the beginning of the pulse; (b)Integrated intensity and Gaussian fit of the OTR image. Note the enhancement at the peak.

codes is still in the development stage in order to properly deposit the particle beam energy and simultaneously model the hydro motion, so no results will be presented.

An electron linear induction accelerator [36, 37] is used to produce a large volume ($3 \times 10^{-4}$ cm$^3$) of WDM that expands adiabatically, which has the potential to provide a longer, stable method of measuring the EOS. We are not claiming this in this letter. There are three parameters we plan to measure for the EOS: temperature, density, and pressure. A 100-ns-long, 1.7 kA electron bunch is accelerated and transported through the induction linac to 19.8 MeV and then is focused onto a 100-$\mu$m-thick Ti foil. The optical diagnostic suite (Fig. 1) including plume imaging, near field optical transition radiation (OTR) [38–42], and visible spectroscopy both orthogonal to the surface and on the target face is presented. This is the first quantitative set of experiments documenting the adiabatic expansion of a warm dense plasma on ∼10-100 ns time scales. We also measure $n_e$ & $T_e$ of the degenerate plasma 200 ns after energy is deposited into thin foils by an intense relativistic electron beam.

## II. COLLISIONAL HEATING & OPTICAL MEASUREMENTS

The collisional heating process is performed by depositing the particle beam energy into the material lattice of the foil and stripping the electrons from the atom. In this case the particles inducing the collisions are relativistic electrons. Since we are operating near the minimum of the electronic stopping power (dE/dx) curve the collisional heating is not optimized [43]. The energy dissipated into these thin (100 $\mu$m) foils is 9.7 J in Ti, assuming a 1-mm radial distribution; $< 0.5\%$ of the available 2.7 kJ in particle beam energy. This is understandable because the range (penetration depth) of relativistic electrons at this kinetic energy is 2.8 cm in Ti, $> 200\times$ our foil thickness. However, it is unnecessary to use thicker foils because the energy is deposited isochorically and we will not achieve any higher temperatures with thicker foils; we will just create more Bremsstrahlung X-ray radiation scattered into our diagnostics, reducing the signal-to-noise ratio.

The current density, J(x,y), is temporally resolved through a near-field OTR measurement [38–42], which is made with an ICCD camera[44]. We state near-field because we are imaging the beam distribution on the surface of the foil as shown in Fig. 2(a) rather than the far-field distribution (at infinity) in which we measure the radiation lobes with polarization. The camera shown in the top of Fig. 1 (shaded in red) is mounted upstream of the vacuum vessel, parallel to the beam axis, and is used with a set of four mirrors to only view the forward scattered OTR at a $20^o$ angle on the back side of the foil. We use the near field approach to determine the peak focus after the 20 ns rise time in the pulse, 30 ns prior to any plasma generation as will be shown below. A sample shot of the peak focus is shown in Fig. 2 with a Gaussian fit to the distribution indicating a = 2.23 mm and FWHM = 2.63 mm, where $a = 2\sigma$.

In addition we simultaneously measure the generation of a target plume indicating an average particle beam density threshold of $\langle n_e \rangle > 10^{17}$ m$^{-3}$ is required to generate an expanding warm dense plasma. Plume expansion measurements are made with two separate cameras. The first is a legacy PI-Max512 ICCD camera [44], capable of resolving down to 5 ns gates with a 16-bit digitization rate. The second camera is a Simacon image intensified fast-framing camera composed of 8 individual ICCDs, capable of taking 2 gated, 12-bit images each (16 total). Each ICCD is capable of resolving down to 5 ns with 1 ns between one camera frame to the next, within a minimum window of 600 ns for all 16 images. The two cameras are mounted external to the diagnostic vacuum

section shown in Fig. 1 (shaded in blue and green). The light is reflected with a single mirror to image the upstream expansion of the plume.

The expansion of a Ti foil heated by the 1.7 kA beam pulse was measured on consecutive shots with the single frame camera in Fig. 3(a). 50 ns into the pulse, ionization becomes visible, the intensity begins to increase slightly with subsequent 20 ns gates, and we see rapid expansion, $\sim$ 1 mm/20 ns. However, this expansion slows down 10$\times$ in the first 100 ns, indicating the expansion is adiabatic, like a point source explosion [1–3]. The shock front or leading edge of the plume is compared to the similarity solution: $z(t) = \eta(Et^2/\rho_o)^{1/5}$, where $\eta$ is a geometric constant, $E$ is the energy deposited into the Ti foil (9.7 J), $t$ is time, and $\rho_o$ is the density of the foil (4510 kg/m$^3$). The rate of expansion of the plume $v(t)$ is simply:

$$v(t) = \frac{dz(t)}{dt} = \frac{2\eta}{5}\left(\frac{E}{\rho_o}\right)^{1/5} t^{-3/5}. \qquad (1)$$

As will be shown below, the experimental measurements we have made with two separate camera systems over multiple shots agrees well with the point source solution for adiabatic expansion. At 110 ns after the beginning of the pulse the intensity increases 5$\times$, where the warm dense plasma begins radiating the most as shown in Fig. 3(b). After that point it continues to expand and cool off as shown with reduced intensity. A radial profile was extracted at 250 $\mu$m intervals providing $\sigma$ vs. the expansion axis (Fig. 3(c)) for each time slice in Fig. 3(a). A sample Gaussian fit at 2.1 mm for the 110 ns gate is also shown (Fig. 3(d)); indicating radial symmetry although there is axial dependence to the expansion, which may be a characteristic of a shock.

A full expansion of Ti was examined on a single shot basis with the fast-framing camera. Several shots were taken to determine the repeatability of the expansion rate of the visible plume with 100 ns and 1 $\mu$s gates (Fig. 4). During the first 100 ns frame the plume is about 1 sq. mm. This is >2$\times$ smaller than the total integrated size measured with the PI-Max camera in Fig. 3. Keep in mind the sensitivity of the pixels in this camera are >10$\times$ less than the PI-Max; the Simacon has 12 bits of dynamic range and the PI-Max has 16 bits. As a result of this reduced range, the gain was minimized on these images and a 5 or 10% transmission neutral density filter was used in order to measure the full dynamic nature of the expansion. On each subsequent frame for the 100 ns data set, the intensity is slightly reduced and the measured plume expansion rate reduces from 3.8-1.0 mm/$\mu$s over the 0.1-1.0 $\mu$s band (Figs. 4(a) & (c)). This agrees pretty well with the similarity solution in Eq. 1, although there are a few outliers. At these time scales (> 100 ns) the plasma has expanded out of the warm dense phase into a moderately coupled, $\Gamma \sim 0.1$, and degenerate $\theta > 10^2$ plasma regime, where we are referring to the Coulomb coupling and the degeneracy ($\theta$ = Thermal Energy/Fermi Energy). At this point we approximate the state of the plasma as an ideal gas; we are currently evaluating the correct EOS for modeling the heating and expansion of these plasmas [33–35].

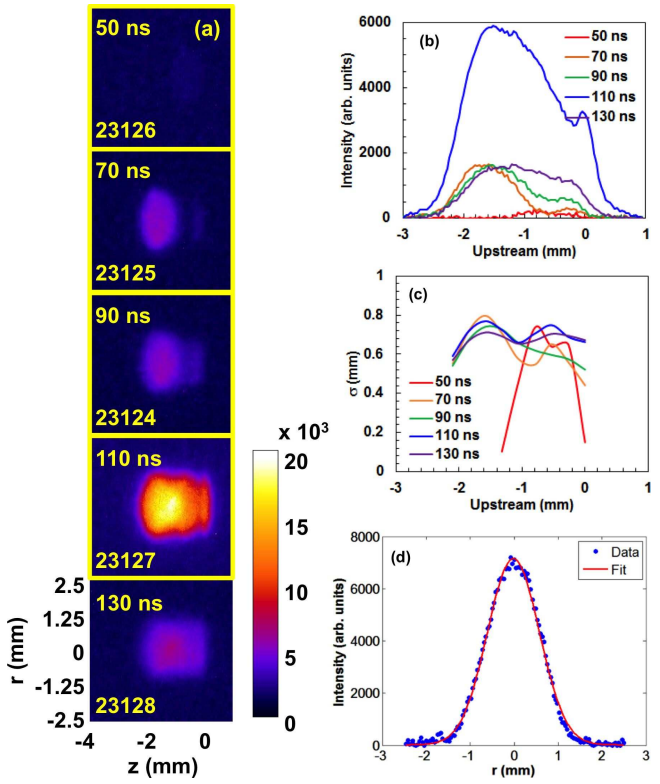


FIG. 3: (a) 20 ns gated images of the expanding plume, the delay after the beginning of the beam pulse and shot number are indicated; (b) Integrated intensity and axial extent of the plume images in (a); (c) plot of $\sigma$ vs. the z-axis for each time slice in (a); and (d) a sample Gaussian fit at 2.1 mm for the 110 ns gate on shot 23127. Note 0 is the upstream side of the target face.

The mean expansion speed for the 100 ns data set is $\sim$1.5 mm/$\mu$s, which corresponds to a calculated Ti temperature of 0.74 eV, target pressure of 6.7$\times$10$^4$ bar and hydrodynamic disassembly time of 31.7 ns from solid density, as shown in the second row of Table I. The measured values are indicated in the table and the remaining unknown values are roughly approximated assuming an ideal gas. The values can be computed from the collisional stopping power $dE/dx$ of a 20 MeV electron beam into 100-$\mu$m-thick Ti foil, where $dE/dx$ = 1.584 MeV-cm$^2$/g. The change in temperature $\Delta T$ (K) is:

$$\Delta T = \frac{q\frac{dE}{dx}}{\pi r^2 C}, \qquad (2)$$

where $q$ is the total electron charge deposited by the electron beam, which is $\sim$140 $\mu$C, $r$ is the beam radius, and $C$ (J/g-K) is the specific heat for the material. The target plasma pressure $P$ (N/m$^2$) can be calculated from the electron density $n_e$ (m$^{-3}$) and temperature (eV): $P$ =

TABLE I: Measured and calculated plasma parameters based on the collisional stopping power (dE/dx) of a 20 MeV electron beam in a radius r. The calculated values are obtained assuming an ideal gas. The measured values are indicated with an "m" superscript.

| r (mm) | $T_e$ (eV) | P (Mbar) | $C_s$ (mm/us) | $t_{hydro}$ (ns) |
|---|---|---|---|---|
| 0.94 | $1.24^m$ | 0.112 | 2.04 | 24.5 |
| 1.20 | 0.74 | 0.067 | $1.57^m$ | 31.7 |
| 1.80 | 0.30 | 0.027 | 1.00 | $50^m$ |

$n_e k_B T$, where $k_B$ is the Boltzmann constant and the temperature conversion of 11604 K/eV is also required. The sound speed expansion of the warm dense plasma is estimated by: $C_s = (\gamma ZP/\rho_o)^{1/2}$, where $\gamma$ is the adiabatic index or isentropic expansion factor ($\gamma = C_p/C_v$), which for our case, a monoatomic metallic plasma is 5/3. $Z$ is the charge state of the plasma and $\rho_o$ is the solid density of the target material. Finally the hydrodynamic disassembly time for expansion on two sides is estimated as: $t_{hydro} = \Delta z/2C_s$, where $\Delta z$ is the target thickness. The plume expands to much larger distributions at a much slower rate when measured with 1 $\mu$s gates (Figs. 4(b) & (c)). These 1 $\mu$s images indicate an overlap with the 100 ns data set, showing a reduced expansion rate from 1.0-0.3 mm/$\mu$s over the 1.0-10 $\mu$s band.

Visible spectroscopy measurements were conducted with a pair of Princeton Instruments Acton spectrometers [45] and PI-Max4 ICCDs [44]. More specific details of this diagnostic are outlined in [46]. The light from the warm dense plasma is coupled into the linear fiber array with a 130-mm lens as shown above in Fig. 1. Fig. 5(a)-(c) illustrates a high resolution measurement (1800 G/mm) of the Ti spectrum measured over a 200 ns period, 300 ns after the beginning of the pulse (or 200 ns after the pulse has ended) on two separate shots. Lower intensity emission has been observed 100 ns earlier. Each shot provided a bandwidth of 8-9 nm, a resolution $< 0.12$ $\mathring{A}$, and the emitted lines are only Ti-I lines. On shot 23115 we measured both emitted and absorbed spectra (Fig. 5 (a)&(b)) on two separate fibers, which appeared to be mirror images in intensity of one-another. On shot 23127 we measured additional emission spectra on a lower band.

The Los Alamos suite of atomic structure and collision codes [48] was used to generate atomic energy levels, wavefunctions, and transition probabilities utilizing the semi-relativistic CATS [49, 50] atomic structure code, available NIST values [51], and the multi-purpose ionization code GIPPER [48, 52]. Plasma modeling calculations were then performed for the neutral, singly, and doubly ionized species of Ti using the Los Alamos ATOMIC code [53, 54] and the atomic data generated from CATS & GIPPER. ATOMIC was run in local-thermodynamic-equilibrium (LTE) mode, which should be a good approximation for the plasma conditions considered here [47, 55]. The emission produced from these modeling calculations is presented in 5(a)&(c). Every line measured in both wavelength bands is reproduced by the calculations and the best-fit estimates for the temperature and density result in $T_e = 1.25$ eV and $n_e = 3 \times 10^{17}$ cm$^{-3}$. This indicates the average density has expanded 5 orders below $\rho_o$, 200 ns after energy deposition.

This measured $T_e$ is used to estimate the heated radius, P, $C_s$, and $t_{hydro}$ at solid density as shown in the first row of Table I; indicating a slightly better deposition of energy than estimated from the expansion images. A comparison to $t_{hydro} = 50$ ns, based on the measurements in Fig. 3, is also shown in the bottom row of Table I to illustrate a colder $T_e = 0.30$ eV. A better spectral fit could be obtained by performing a detailed radiation transport model that incorporates the spatial temperature and density distribution and the opacity of each spectral line [56]. However, this requires a time resolved density gradient measurement and a detailed hydro model which we are currently developing.

## III. CONCLUSIONS

We confirmed we produce a large volume of adiabatically expanding warm dense plasma through isochoric heating with an electron beam $\langle n_e \rangle > 10^{17}$ m$^{-3}$, $< 10^{10}$ of solid density Ti. We developed a spatial and temporal profile of the expanding plasma off the target surface, which agrees well with the point source solution and for multiple diagnostics. The spatial distributions are extremely reproducible for identical incoming beam parameters. Visible expansion of the plume does not begin until ~50 ns into the beam pulse and the peak intensity is observed near the end of energy deposition.

Visible emission and absorption lines of Ti-I are only observed >100-200 ns after energy is deposited, once the plasma has adiabatically expanded and cooled into a degenerate plasma. The LANL ATOMIC code is able to reproduce the spectra to first order and provide a measured $T_e = 1.25$ eV and $n_e = 3 \times 10^{17}$ cm$^{-3}$, which indicates a slightly higher temperature than what was estimated by the expansion measurements with the ICCD cameras. This confirms we are not measuring the EOS in warm dense phase. We are still deploying additional density and X-ray diagnostics to characterize the temperature and density of the WDM at early times ($< 100$ ns). We are also evaluating the correct EOS for modeling the heating and expansion of these plasmas. In addition we wish to measure the expansion velocity of the foil and a disassembly time with a PDV probe. Each of these should help provide a conclusive measurement of how long the warm dense phase lasts with this heating method and a map of the EOS across a density range of $10^{16} < n_e$ (cm$^{-3}$) $< 10^{23}$.

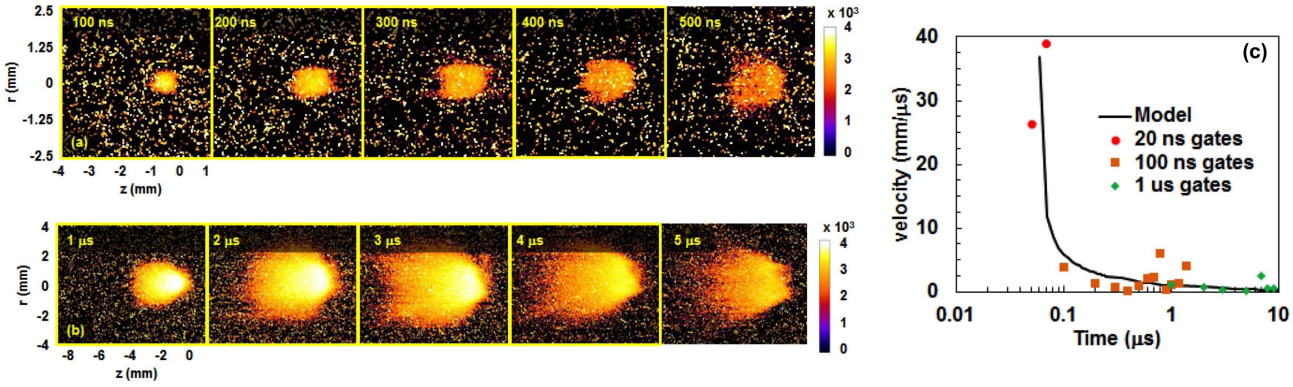


FIG. 4: (a)100 ns gated images of the expanding plume and the delay after the beginning of the pulse is indicated, shot number 23103; (b)1 $\mu$s gated images of the expanding plume and gate with respect to the beginning of the pulse is indicated, shot number 23105 (note scale differences). Images are shown on log scale to indicate full expansion; (c) velocity profile from multiple 20 ns (red), 100 ns (orange), and 1 $\mu$s (green) gated images with the PI-Max512 and Simacon fast-framing cameras. The black line is the point source solution from Eq. 1.

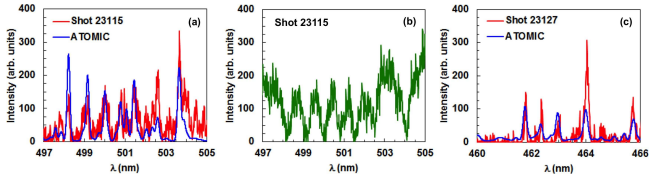


FIG. 5: Measured Ti-I spectra over a 200 ns gate for shot 23115 indicating (a) emission; and (b) absorption over the 496-506 nm band; and (c) emission for shot 23127 over the 454-466 nm band. The comparison of the ATOMIC fit calculation is shown in blue.


### Acknowledgments

This work was supported by the National Nuclear Security Administration of the U.S. Department of Energy under Contract No. DE-AC52-06NA25396. We would like to thank M. Berninger, C.A. Ekdahl, and M.E. Schulze for their technical discussions. We would like to take the opportunity to thank Don Roeder, Valerie Fatherley, Anthony Chavez, and Sharon Dominguez for their manufacturing and design support. We would like to thank the operators, technicians, students and engineers Sam Snider, Jules Carson, Josh Esquibel, Geronimo Gonzalez, Robbie Brooks, Melissa Reed, Tim McCurdy, Rudy Valdez, Armando Martinez, Tim Rushenberg, Nick Ramey, and Travis Weaver for their continued support.



[1] H.A. Bethe, K. Fuchs, J.O. Hirschfelder, J.L. Magee, R.E. Peierls, and J. von Neumann, "BLAST WAVE", Los Alamos Report LA-2000, Ch.2, (1947).
[2] G.I. Taylor, Proc. Roy. Soc. A **201**, 159 (1950).
[3] G.I. Taylor, Proc. Roy. Soc. A **201**, 175 (1950).
[4] A.L. Kritcher et al., Phys. Plasmas, **16**, 056308 (2009).
[5] A.L. Kritcher, P. Neumayer, C.R.D. Brown, P. Davis, T. Döppner, R.W. Falcone, D.O. Gericke, G. Gregori, B. Holst, O.L. Landen, H.J. Lee, E.C. Morse, A. Pelka, R. Redmer, Phys. Rev. Lett., **103**, 245004 (2009).
[6] L.B. Fletcher, A.L. Kritcher, A. Pak, T. Ma, T. Döppner, C. Fortmann, L. Divol, O.S. Jones, O.L. Landen, H.A. Scott, J. Vorberger, D.A. Chapman, D.O. Gericke, B.A. Mattern, G.T. Seidler, G. Gregori, R.W. Falcone, and S.H. Glenzer, Phys. Rev. Lett., **112**, 145004 (2014).
[7] A. Levy, P. Audebert, R. Shepherd, J. Dunn, M. Cammarata, O. Ciricosta, F. Deneuville, F. Dorchies, M. Fajardo, C. Fourment, D. Fritz, J. Fuchs, J. Gaudin, M. Gauthier, A. Graf, H. J. Lee, H. Lemke, B. Nagler, J. Park, O. Peyrusse, A. B. Steel, S. M. Vinko, J. S. Wark, G. O. Williams, D. Zhu, and R. W. Lee Phys. Plasmas **22**, 030703 (2015).
[8] J. Cihelka, L. Juha, J. Chalupsk, F.B. Rosmej, O. Renner, K. Saksl, V. Hjkov, L. Vyn, E. Galtier, R. Schott, A.R. Khorsand, D. Riley, T. Dzelzainis, A.J. Nelson, R.W. Lee, P.A. Heimann, B. Nagler, S. Vinko, J. Wark, T. Whitcher, S. Toleikis, T. Tschentscher, R. Fustlin, H. Wabnitz, S. Bajt, H. Chapman, J. Krzywinski, R. Sobierajski, D. Klinger, M. Jurek, J. Pelka, S. Hau-Riege, R.A. London, J. Kuba, N. Stojanovic, K. Sokolowski-Tinten, A.J. Gleeson, M. Strmer, J. Andreasson, J. Hajdu, B. Iwan, and N. Timneanu, Proc. of SPIE, **7361** (2009).
[9] A.L. Kritcher, T. Doeppner, D. Swift, J. Hawreliak, J. Nilsen, J. Hammer, B. Bachmann, G. Collins, O. Lan-

den, C. Keane, S. Glenzer, S. Rothman, D. Chapman, D. Kraus, and R.W. Falcone, Journal of Physics: Conference Series **688**, 012055 (2016).
[10] T. Ao, E.C. Harding, J.E. Bailey, R.W. Lemke, M.P. Desjarlais, S.B. Hansen, I.C. Smith, M. Geissel, A. Maurer, J. Reneker, D. Romero, D.B. Sinars, G.A. Rochau, and J.F. Benage, High Energy Density Phys. **18**, 26 (2016).
[11] P.F. Knapp, S.A. Pikuz, T.A. Shelkovenko, D.A. Hammer, and S. B. Hansen, Phys. Plasmas **19**, 056302 (2012).
[12] N.A. Tahir et al., Laser Part. Beams **22**, 485 (2004).
[13] A. Tauschwitz, J.A. Maruhn, D. Riley, F.B. Rosmej, S. Borneis, A. Tauschwitz, and K. Witte, Journal of Physics: Conference Series **112**, 032074 (2008).
[14] P.A. Ni, M.I. Kulish, V. Mintsev, D.N. Nikolaev, V.YA. Ternovoi, D.H.H. Hoffmann, S. Udrea, A. Hug, N.A. Tahir, and D. Varentsov, Laser and Particle Beams **26**, 583 (2008).
[15] J.E. Coleman, Ph.D. Thesis, University of California, Berkeley, 2008.
[16] F.M. Bieniosek, J.J. Barnard, A. Friedman, E. Henestroza, J.Y. Jung, M.A. Leitner, S. Lidia, B.G. Logan, R.M. More, P.A. Ni, P.K. Roy, P.A. Seidl, W.L. Waldron, Journal of Physics: Conference Series **244**, 032028 (2010).
[17] P.A. Ni, F.M. Bieniosek, E. Henestroza, S.M. Lidia, Nucl. Instrum. Methods Phys. Res., Sect. A **733**, 12 (2014).
[18] P.A. Seidl, A. Persaud, W.L. Waldron, J.J. Barnard, R.C. Davidson, A. Friedman, E.P. Gilson, W.G. Greenway, D.P. Grote, I.D. Kaganovich, S.M. Lidia, M. Stettler, J.H. Takakuwa, T. Schenkel, Nucl. Instrum. Methods Phys. Res., Sect. A **800**, 98 (2015).
[19] P.A. Seidl, J.J. Barnard, R.C. Davidson, A. Friedman, E.P. Gilson, D. Grote, Q. Ji, I.D. Kaganovich, A. Persaud, W.L. Waldron, and T. Schenkel, Journal of Physics: Conference Series **717**, 012079 (2016).
[20] P.A. Seidl, private communication.
[21] A. Pelka, G. Gregori, D.O. Gericke, J. Vorberger, S.H. Glenzer, M.M. Gunther, K. Harres, R. Heathcote, A.L. Kritcher, N.L. Kugland, B. Li, M. Makita, J. Mithen, D. Neely, C. Niemann, A. Otten, D. Riley, G. Schaumann, M. Schollmeier, An. Tauschwitz, and M. Roth, Phys. Rev. Lett., **105**, 265701 (2010).
[22] W. Bang, B.J. Albright, P.A. Bradley, D.C. Gautier, S. Palaniyappan, E.L. Vold, M.A. Santiago Cordoba, C.E. Hamilton, and J.C. Fernndez, Sci. Rep. **5**, 14318 (2015).
[23] W. Bang, B.J. Albright, P.A. Bradley, E.L. Vold, J.C. Boettger, and J.C. Fernandez, Phys. Rev. E **92**, 063101 (2015).
[24] M. Gittings, R. Weaver, M. Clover, T. Betlach, N. Byrne, R. Coker, E. Dendy, R. Hueckstaedt, K. New, W.R. Oakes, D. Ranta, and R. Stefan, The RAGE radiation-hydrodynamic code, Comput. Sci. Disc. **1**, 015005 (2008).
[25] S.P. Lyon and J.D. Johnson, Sesame: The los alamos national laboratory equation of state database. Los Alamos National Laboratory Report No. LA-UR-92-3407 (1992).
[26] G. Hairapetian, P. Davis, C.E. Clayton, C. Joshi, S.C. Hartman, C. Pellegrini, and T. Katsouleas, Phys. Rev. Lett. **72**, 2403 (1994).
[27] G. Hairapetian, P. Davis, C.E. Clayton, C. Joshi, C. Pellegrini, and T. Katsouleas, Phys. Plasmas, **2**, 2555 (1995).
[28] C. Joshi, B. Blue, C.E. Clayton, E. Dodd, C. Huang, K.A. Marsh, W.B. Mori, S. Wang, M.J. Hogan, C. OConnell, R. Siemann, D. Watz, P. Muggli, T. Katsouleas, and S. Lee., Phys. Plasmas, **9**, 1845 (2002).
[29] C. Vermare, H.A. Davis, D.C. Moir, and T.P. Hughes, Phys. Plasmas **10**, 277 (2003).
[30] S. Sampayan, R. Buckles, G. Caporaso, F. C. Chambers, Y-J Chen, S. Falabella, F. Goldin, G. Guethlein, D. Ho, M. Heino, T. Houck, E. Lauer, J. McCarrick, R. Neurath, P. Pincosy, R. Richardson, D. Sanders, and J. Weir in Proceedings of the Particle Accelerator Conference, Chicago, 2001, p. 330.
[31] D.R. Welch and T.P. Hughes, Laser and Particle Beams, **16**, 285 (1998).
[32] B.V. Oliver, D.R. Welch, and T.P. Hughes, Beam-target interactions in single and multi-pulse radiography, MRC/ABQ-R-1909 Report, 1999.
[33] M.J. Berninger and T. Kwan, private communication.
[34] M.L. Klasky, private communication.
[35] D.R. Welch and C.L. Miller, private communication.
[36] J.E. Coleman, D.C. Moir, C.A. Ekdahl, J.B. Johnson, B.T. McCuistian, G.W. Sullivan, and M.T. Crawford, Phys. Rev. ST Accel. Beams **17**, 030101 (2014).
[37] J.E. Coleman, C.A. Ekdahl, D.C. Moir, G.W. Sullivan, and M.T. Crawford, Phys. Rev. ST Accel. Beams **17**, 092802 (2014).
[38] L. Wartski, S. Roland, J. Lasalle, M. Bolore, and G. Filippi J. Appl. Phys. **46**, 3644 (1975);
[39] C.B. Reid, Masters Thesis, Naval Postgraduate School, Monterey, CA (1990).
[40] B. Gitter, CAA Tech Note 24, (1992).
[41] R.B. Fiorito and D.W. Rule, AIP Conference Proceedings **319**, 21 (1994).
[42] P. Karataev, A. Aryshev, S. Boogert, D. Howell, N. Terunuma, and J. Urakawa, Phys. Rev. Lett. **107**, 174801 (2011).
[43] See physics.nist.gov/cgi-bin/Star/e_table.pl for information about dE/dx.
[44] See http://www.princetoninstruments.com/products/imcam /pimax/ for information about PI-Max cameras.
[45] See http://www.princetoninstruments.com/products/spec /actonseries/ for information about Acton Spectrometers.
[46] J.E. Coleman, Rev. Sci. Instrum. **87**, 123113 (2016).
[47] J. Colgan, E.J. Judge, D.P. Kilcrease, and J.E. Barefield II, Spectrochim. Acta Part B **97**, 65 (2014).
[48] C.J. Fontes, H.L. Zhang, J. Abdallah Jr, R.E.H. Clark, D.P. Kilcrease, J. Colgan, R.T. Cunningham, P. Hakel, N.H. Magee, and M.E. Sherrill, The Los Alamos suite of relativistic atomic physics codes, J. Phys. B **48** 144014 (2015).
[49] R.D. Cowan, The Theory of Atomic Structure and Spectra, (University of California Press, Berkeley, 1981).
[50] J. Abdallah, R.E.H. Clark, R.D. Cowan, CATS: Cowan atomic structure code, Los Alamos National Laboratory, Los Alamos Manual No. LA 11436-M-I (1988).
[51] A. Kramida, Y. Ralchenko, and J. Reader, NIST ASD Team 2014 NIST Atomic Spectra Database v 5.2. See http://physics.nist.gov/PhysRefData/ASD /lines_form.html for information about documented Ti-I lines.
[52] R.E.H. Clark, J. Abdallah Jr, J.B. Mann, Integral and differential cross sections for electron impact ionization, Ap. J. **381** 597 (1991).
[53] N.H. Magee, J. Abdallah, J. Colgan, P. Hakel, D.P. Kilcrease, S. Mazevet, M. Sherrill, C.J. Fontes, H.L. Zhang, Los Alamos Opacities: Transition from LEDCOP to

ATOMIC, 14th Topical Conference on Atomic Processes in Plasmas, (Eds: J.S. Cohen, S. Mazevet, D.P. Kilcrease, AIP Conference Proceedings, New York, 2004) 168-179.
[54] P. Hakel, M.E. Sherrill, S. Mazevet, J. Abdallah Jr., J. Colgan, D.P. Kilcrease, N.H. Magee, C.J. Fontes, and H.L. Zhang, The new Los Alamos Opacity Code ATOMIC, J. Quant. Spectr. Rad. Transfer **99** 265 (2006).
[55] R.W.P. McWhirter, Plasma diagnostic techniques, Academic Press, New York, 1965.
[56] P. Hakel, Comput. Phys. Commun. **207**, 415 (2016).